nature structural & molecular biology

Transfer RNA–mediated regulation of ribosome dynamics during protein synthesis

Jingyi Fei[1,3], Arianne C Richard[2,3], Jonathan E Bronson[1,3] & Ruben L Gonzalez Jr[1]

Translocation of tRNAs through the ribosome during protein synthesis involves large-scale structural rearrangement of the ribosome and ribosome-bound tRNAs that is accompanied by extensive and dynamic remodeling of tRNA-ribosome interactions. How the rearrangement of individual tRNA-ribosome interactions influences tRNA movement during translocation, however, remains largely unknown. To address this question, we used single-molecule FRET to characterize the dynamics of ribosomal pretranslocation (PRE) complex analogs carrying either wild-type or systematically mutagenized tRNAs. Our data reveal how specific tRNA-ribosome interactions regulate the rate of PRE complex rearrangement into a critical, on-pathway translocation intermediate and how these interactions control the stability of the resulting configuration. Notably, our results suggest that the conformational flexibility of the tRNA molecule has a crucial role in directing the structural dynamics of the PRE complex during translocation.

During the elongation stage of protein synthesis, ribosome-catalyzed addition of each amino acid to the nascent polypeptide chain is followed by the rapid and unidirectional translocation of the tRNA–mRNA complex through the ribosome by precisely one codon. Translocation occurs through a multistep process that requires extensive remodeling of tRNA-ribosome interactions and substantial structural distortions of the ribosome-bound tRNAs relative to the 'ground state' structures of ribosome-free tRNAs[1–3]. Despite the fundamental importance of translocation to protein synthesis, how the ribosome physically coordinates, regulates and executes this process remains poorly understood.

Recently, single-molecule fluorescence resonance energy transfer (smFRET) studies have shown that deacylation of the peptidyl tRNA bound within the ribosomal peptidyl tRNA–binding (P) site during peptide bond formation enables thermally activated and stochastic structural fluctuations of the resulting PRE complexes[4–9]. These complexes, carrying deacylated tRNA at the P site and peptidyl tRNA at the aminoacyl-tRNA binding (A) site, oscillate between two major global conformational states. In global state 1 (GS1), the small and large (30S and 50S, respectively, in *Escherichia coli*) ribosomal subunits are in their nonrotated intersubunit orientation, the tRNAs are positioned in their classical 30S P site/50S P site (P/P) and A/A configurations, and the ribosomal L1 stalk is in its open conformation; in global state 2 (GS2), the ribosomal subunits are in their rotated intersubunit orientation, the tRNAs are positioned in their hybrid P/E (where 'E' denotes the ribosomal exit site, or deacylated tRNA–binding site) and A/P configurations, and the L1 stalk is in its closed conformation[5] (**Fig. 1a**). Biochemical data support the view that GS2 is an on-pathway intermediate in translocation[10] and smFRET studies have shown that binding of elongation factor G (EF-G) to the PRE complex markedly shifts the GS1↔GS2 dynamic equilibrium toward GS2 as part of the mechanism through which it promotes translocation[5–8,11]. Moreover, pre–steady state smFRET studies have suggested that the GS1→GS2 transition may limit the rate at which EF-G can productively bind and act on the PRE complex to promote translocation[6]; this has recently been confirmed[12].

A key regulator of both the GS1↔GS2 equilibrium and translocation is the P-site tRNA. Indeed, the ability of the elongating ribosome to actuate the GS1↔GS2 equilibrium[6–8,13–15] and trigger the productive binding of EF-G[16,17] that leads to stabilization of GS2[6–8,11,18,19], ribosome-stimulated GTP hydrolysis[16,17] and ultimately translocation[17,20] depends critically on the presence of a full-length, deacylated P-site tRNA. In addition to the presence and acylation state of the P-site tRNA, the GS1↔GS2 equilibrium and translocation are sensitive to the identity of this tRNA, indicating that specific P-site tRNA-ribosome interactions and/or tRNA structural features unique to each tRNA can differentially modulate the GS1↔GS2 equilibrium and translocation. In the most extensively investigated examples, smFRET studies have shown that, relative to PRE_{Phe} complexes (where 'Phe' denotes a P-site $tRNA^{Phe}$), PRE_{fMet} complexes have a GS1↔GS2 equilibrium that is inherently shifted toward GS1 (refs. 6–8,10,14,15) and, upon EF-G binding, is shifted toward GS2 through a kinetic mechanism distinct from that observed in PRE_{Phe} complexes[7]. Correspondingly, PRE_{fMet} complexes have a slower rate of translocation than analogous PRE complexes carrying elongator P-site tRNAs[10,20].

It is not yet known, however, which tRNA-ribosome interactions or aspects of tRNA structure lead to tRNA-mediated regulation of the GS1↔GS2 equilibrium and translocation. In this study,

[1]Department of Chemistry, Columbia University, New York, New York, USA. [2]Department of Biological Sciences, Columbia University, New York, New York, USA. [3]Present addresses: Department of Physics, Center for the Physics of Living Cells, University of Illinois at Urbana-Champaign, Urbana, Illinois, USA (J.F.); Immunoregulation Section, Autoimmunity Branch, National Institute of Arthritis and Musculoskeletal and Skin Diseases, Bethesda, Maryland, USA (A.C.R.); Boston Consulting Group, New York, New York, USA (J.E.B.). Correspondence should be addressed to R.L.G. (rlg2118@columbia.edu).

Received 9 December 2010; accepted 14 June 2011; published online 21 August 2011; doi:10.1038/nsmb.2098

we investigated how tRNAs regulate the GS1↔GS2 equilibrium by using smFRET to compare the kinetic differences among PRE complexes carrying wild-type and strategically mutated tRNAs. We started by comprehensively characterizing the GS1↔GS2 equilibrium with and without EF-G in PRE complexes carrying an expanded set of wild-type tRNAs at the P site. We show that, relative to all the elongator tRNAs we examined, $tRNA^{fMet}$ uniquely modulates the GS1↔GS2 equilibrium and the ability of EF-G to shift this equilibrium toward GS2. After these initial experiments, we examined a series of PRE complexes carrying $tRNA^{fMet}$ mutants, in which sequence elements unique to $tRNA^{fMet}$ were mutated to the corresponding sequences in elongator $tRNA^{Phe}$, at the P site. Our studies collectively show that the kinetics of the GS1↔GS2 equilibrium and the ability of EF-G to shift this equilibrium toward GS2 are at least partly dictated by the intrinsic conformational flexibility of the tRNA as well as by specific tRNA-ribosome interactions. Specifically, our results suggest that the GS1→GS2 transition rate is primarily determined by the intrinsic conformational flexibility of the P-site tRNA itself, whereas the GS2→GS1 transition rate is largely determined by the minor groove–minor groove interaction between the aminoacyl acceptor stem of the P/E tRNA and helix H68 of 23S rRNA at the 50S subunit E site. Our proposal that the intrinsic conformational flexibility of the P-site tRNA can modulate the GS1→GS2 transition rate suggests that the ease with which the ribosome can distort the tRNA structure is an important aspect of translocation. This expands the functionally important role of tRNA deformability during translation elongation beyond that already proposed for aminoacyl-tRNA (aa-tRNA) selection[21–23]. We hypothesize that the differences observed in the dynamics of PRE complexes carrying initiator versus elongator tRNAs in the P site derive from the distinct evolutionary pressures that have been imposed on these tRNAs for optimal performance during the initiation and elongation stages of protein synthesis, respectively.

RESULTS

An intraribosomal smFRET signal reports on GS1↔GS2

Fluctuation of the L1 stalk between open and closed conformations is one of the defining features of the GS1↔GS2 equilibrium[6,7,9] (**Fig. 1a**). We have previously developed and validated a doubly fluorescently labeled 50S subunit (harboring a Cy5 acceptor fluorophore within ribosomal protein L1 and a Cy3 donor fluorophore within ribosomal protein L9) that yields an smFRET signal sensitive to fluctuations of the L1 stalk between open and closed conformations[7] (**Fig. 1b** and **Supplementary Methods**). Using these doubly labeled 50S subunits, unlabeled 30S subunits, a set of natural, deacylated *E. coli* tRNAs and a corresponding set of mRNAs (**Supplementary Fig. 1**), we nonenzymatically prepared two PRE^{-A}_{fMet} complexes (where '–A' denotes a PRE complex analog in which the peptidyl tRNA is absent from the A site) and four PRE^{-A}_{elong} complexes (where 'elong' denotes an elongator P-site tRNA; **Fig. 1c**). The two PRE^{-A}_{fMet} complexes carried one of the two isoacceptors of $tRNA^{fMet}$: $tRNA^{fMet}_1$, which is encoded by the *metZ* gene ($PRE^{-A}_{fMet\text{-}1}$), or $tRNA^{fMet}_2$, which is encoded by the *metY* gene ($PRE^{-A}_{fMet\text{-}2}$)[24]. The four PRE^{-A}_{elong} complexes carried either $tRNA^{Phe}$ (PRE^{-A}_{Phe}), $tRNA^{Tyr}$ (PRE^{-A}_{Tyr}), $tRNA^{Glu}$ (PRE^{-A}_{Glu}) or $tRNA^{Val}$ (PRE^{-A}_{Val}). All six PRE^{-A} complexes were imaged using total internal reflection fluorescence (TIRF) microscopy (see Online Methods and **Supplementary Methods** for details on sample preparation and TIRF imaging).

Consistent with earlier results[7], each PRE^{-A} complex has two FRET states centered at FRET efficiencies of 0.56 ± 0.02 and 0.36 ± 0.01, corresponding to the open and closed conformations of the L1 stalk and reporting on GS1 and GS2, respectively. Also, as reported earlier[7], the smFRET-versus-time trajectories partition into three subpopulations depending on whether the complexes exclusively occupy GS1 (SP_{GS1}), exclusively occupy GS2 (SP_{GS2}) or fluctuate between GS1 and GS2 (SP_{fluct}) before fluorophore photobleaching (**Fig. 2**). PRE^{-A} complexes carrying different P-site tRNAs had unique population distributions between the open and closed L1 stalk conformations (**Fig. 3**). Notably, the tRNA-dependent trend in K_{eq} values for the equilibrium between the open and closed L1 stalk conformations (**Table 1**) in $PRE^{-A}_{fMet\text{-}1}$, PRE^{-A}_{Phe} and PRE^{-A}_{Tyr} mirrors the tRNA-dependent trend observed earlier[8] in K_{eq} values for the equilibrium between the nonrotated and rotated intersubunit orientations in the analogous PRE^{-A} complexes. This observation supports a model in which the open and closed conformations of the L1 stalk are coupled to the nonrotated and rotated intersubunit orientations of the ribosome, respectively, within the GS1↔GS2 equilibrium[5,6] (see **Supplementary Discussion**).

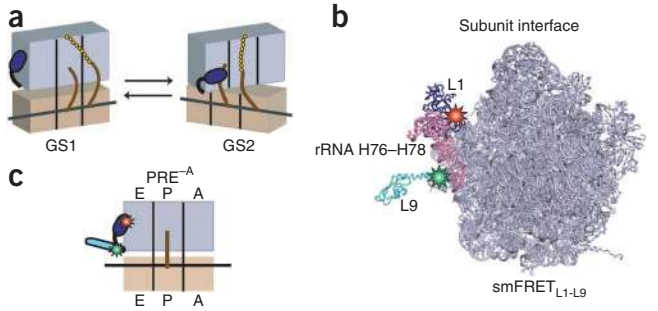

Figure 1 Global states model of the PRE complex, L1-L9 labeling strategy and PRE^{-A} complexes. (**a**) Cartoon diagram of global states model of PRE complex. The 30S and 50S subunits, tan and lavender, respectively; L1 stalk, dark blue. tRNAs, brown curves; nascent polypeptide, chain of gold spheres. (**b**) Labeling strategy for $smFRET_{L1\text{-}L9}$. The 50S subunit is shown from the perspective of the intersubunit space[31] (PDB 2J01). L1 stalk consists of 23S rRNA helices 76–78 (pink) and r-protein L1 (dark blue). r-protein L9, cyan. Donor (Cy3) and the acceptor (Cy5) fluorophores are green and red stars on r-proteins L9 and L1, respectively. Image was rendered using PyMol[50]. (**c**) Cartoon diagram of a PRE^{-A} complex. PRE^{-A} complexes are formed using an L1-L9 labeled 50S subunit and carry a deacylated P-site tRNA.

PRE^{-A}_{fMet} complexes have distinct GS1↔GS2 dynamics

Relative to all four PRE^{-A}_{elong} complexes we examined, the two PRE^{-A}_{fMet} complexes had a higher occupancy of GS1 (**Figs. 2b** and **3** and **Table 1**). These results expand upon earlier smFRET[7,8] and biochemical[10,14] studies, suggesting a general distinction between the dynamics of PRE complexes carrying initiator versus elongator tRNAs. Dwell-time analyses of the smFRET data (see Online Methods and **Supplementary Methods**) reveal the kinetic mechanism underlying this difference, indicating that the higher occupancy of GS1 shown by the $PRE^{-A}_{fMet\text{-}1}$ complex relative to the PRE^{-A}_{elong} complexes is driven almost exclusively by a two- to three-fold faster rate of GS2→GS1 transitions ($k_{GS2\rightarrow GS1}$), with almost no effect on the rate of GS1→GS2 transitions ($k_{GS1\rightarrow GS2}$; **Table 1**). For the $PRE^{-A}_{fMet\text{-}2}$ complex, the two- to three-fold faster $k_{GS2\rightarrow GS1}$ observed in the $PRE^{-A}_{fMet\text{-}1}$ complex is further augmented by a 30–70% slower $k_{GS1\rightarrow GS2}$ relative to the PRE^{-A}_{elong} complexes (**Table 1**).

Consistent with earlier reports, binding of EF-G to $PRE^{-A}_{fMet\text{-}1}$ and $PRE^{-A}_{fMet\text{-}2}$ complexes in the presence of the nonhydrolyzable GTP analog guanosine 5′-(β,γ-imido)triphosphate (GDPNP) shifted the GS1↔GS2 equilibrium toward GS2 (**Fig. 3**)[6–8,11]. This was driven primarily by a three- to six-fold increase in $k_{GS1\rightarrow GS2}$ and augmented by a smaller, 30% decrease in $k_{GS2\rightarrow GS1}$ (**Table 1**), thus yielding more frequent fluctuations between GS1 and GS2 relative to $PRE^{-A}_{fMet\text{-}1}$ in the absence of EF-G(GDPNP)[7,11] (**Fig. 2b**). In contrast, binding of EF-G(GDPNP)

to all four PRE$^{-A}_{elong}$ complexes led to a strong stabilization of GS2, corresponding to a large reduction in $k_{GS2\rightarrow GS1}$, so that fluctuations toward GS1, should they occur, were either too rare and/or fast to be observed within our detection limits (**Figs. 2b** and **3**). Confirming our and others' earlier suggestions[7,8,11], these data demonstrate that the presence of tRNA^{fMet} at the P site of PRE complexes distinctly regulates the effect of EF-G binding on the kinetics of GS1→GS2 and GS2→GS1 transitions.

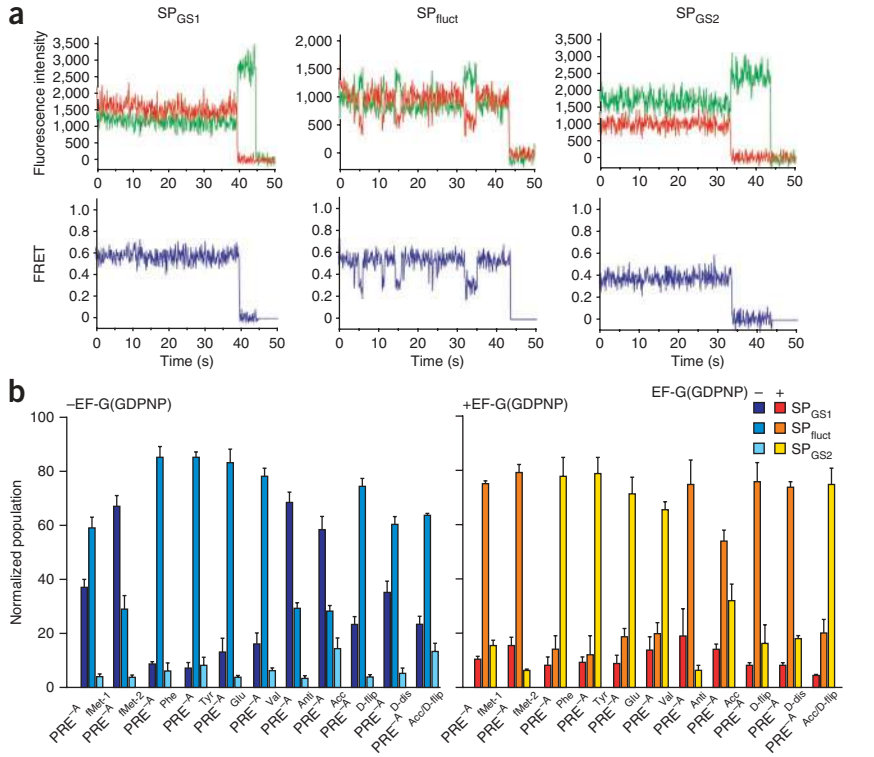

Figure 2 Sample smFRET versus time trajectories and relative occupancies of smFRET trajectory subpopulations. (**a**) Sample smFRET versus time trajectories. Three subpopulations of smFRET trajectories were observed. The first subpopulation, SP$_{GS1}$ (left), shows a stable FRET state centered at 0.56 ± 0.02; the second subpopulation, SP$_{fluct}$ (middle), fluctuates between two FRET states centered at 0.56 ± 0.02 and 0.36 ± 0.01; and the third subpopulation, SP$_{GS2}$ (right), shows a stable FRET state centered at 0.36 ± 0.01. Representative Cy3 and Cy5 emission intensity versus time trajectories, green and red, respectively (top row). Corresponding smFRET versus time trajectories, calculated using $E = I_{Cy5} / (I_{Cy3} + I_{Cy5})$, where E is the FRET efficiency at each time point and I_{Cy3} and I_{Cy5} are emission intensities of Cy3 and Cy5, respectively, are in blue (bottom row). (**b**) Relative occupancies of the three subpopulations of smFRET trajectories. Percentage of smFRET trajectories occupying SP$_{GS1}$, SP$_{fluct}$ and SP$_{GS2}$ for each PRE^{-A} complex without (left) and with (right) EF-G(GDPNP). Data are mean ± s.d. of three independent measurements (see **Supplementary Table 1**).

Generation of tRNA^{fMet} mutants

We next sought to determine whether tRNA structural features unique to tRNA^{fMet} cause P-site tRNA^{fMet} to differentially regulate the GS1↔GS2 equilibrium. Comparative sequence analysis of bacterial tRNAs revealed the existence of three such structural features[25–27]: (i) three consecutive G-C base pairs within the anticodon stem of tRNA^{fMet} that we encountered in <1% of elongator tRNAs; (ii) a mismatched base pair between nucleotides 1 and 72 of the aminoacyl acceptor stem of tRNA^{fMet} that is a Watson-Crick base pair in elongator tRNAs and (iii) a purine-pyrimidine base pair between nucleotides 11 and 24 of the D stem of tRNA^{fMet} that is flipped to a pyrimidine-purine base pair in elongator tRNAs. Biochemical and structural studies have shown that these three features of tRNA^{fMet} are specifically recognized by methionyl-tRNA transformylase and by translation initiation and elongation factors for effective discrimination of tRNA^{fMet} from elongator tRNAs. This ensures proper biosynthesis and selection of fMet-tRNA^{fMet} at the start codon during translation initiation and prevents its incorporation at internal AUG codons during translation elongation[26–29]. Because the regions of the P site–bound tRNA containing these three features all establish extensive interactions with the ribosome that are remodeled during GS1→GS2 and GS2→GS1 transitions[30–33], we reasoned that the divergent dynamic behavior we observed in PRE$^{-A}_{fMet}$ complexes may originate from one or more of these three tRNA^{fMet} structural elements. To determine how each of these structural features of tRNA^{fMet} contributes to the GS1↔GS2 equilibrium, we initially designed three tRNA$^{fMet}_2$ mutants by changing each of its features to the corresponding features in tRNA^{Phe}: (i) a lower anticodon stem G31A C39U mutant (tRNA^{Anti}); (ii), an aminoacyl acceptor stem C1G A72C mutant (tRNA^{Acc}); and (iii) a D stem purine-pyrimidine flip A11C U24G mutant (tRNA$^{D\text{-}flip}$) (**Fig. 4**, Online Methods, **Supplementary Methods** and **Supplementary Figs. 2–5**).

Disruption of anticodon stem does not affect GS1↔GS2

The occupancies of GS1 and GS2 for PRE$^{-A}_{Anti}$ complexes were not substantially altered relative to PRE$^{-A}_{fMet-2}$ complexes (compare **Figs. 3b** and **5a**; see also **Fig. 2b** and **Table 1**). Moreover, $k_{GS1\rightarrow GS2}$ and $k_{GS2\rightarrow GS1}$ for PRE$^{-A}_{Anti}$ complexes with and without EF-G(GDPNP) were within the uncertainty of those for PRE$^{-A}_{fMet-2}$ complexes under the same conditions (**Table 1**). These results demonstrate that the GS1↔GS2 dynamics observed in PRE$^{-A}_{fMet}$ complexes do not arise from the highly conserved consecutive G-C base pairs within the anticodon stem of tRNA^{fMet}. More generally, these results suggest that the GS1↔GS2 equilibrium is relatively insensitive to the identity of the lower anticodon stem base pairs of the tRNA within the P site of the 30S subunit. This observation is consistent with biochemical data[13] and with comparative structural analysis of X-ray crystallographic structures and cryo-EM reconstructions of GS1- and GS2-like ribosomal complexes[30–33], all of which indicate that the transition of the P-site tRNA from the P/P to the P/E configuration predominantly remodels interactions between the P-site tRNA and the 50S subunit, leaving interactions between the anticodon stem of the P-site tRNA and the 30S subunit relatively unaltered (**Fig. 6a**).

5′-terminal base-pairing in acceptor stem lowers $k_{GS2\rightarrow GS1}$

Relative to PRE$^{-A}_{fMet-2}$ complexes, PRE$^{-A}_{Acc}$ complexes have a GS1↔GS2 equilibrium that is shifted toward GS2 (**Figs. 2b**, **3b** and **5b** and **Table 1**). Although $k_{GS1\rightarrow GS2}$ and $k_{GS2\rightarrow GS1}$ are both decreased by conversion of the mismatched C1•A72 base pair within

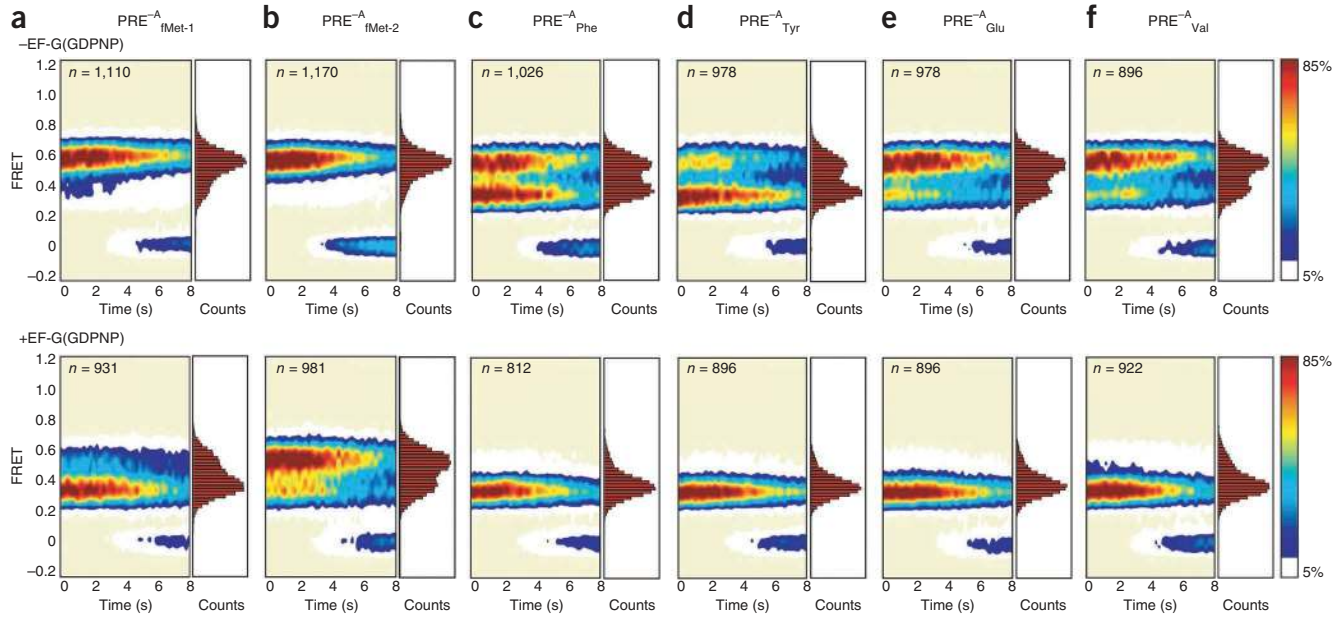

Figure 3 Steady-state smFRET measurements of PRE^{-A} complexes carrying wild-type and elongator tRNAs. Surface contour plots of time evolution of population FRET were generated by superimposing individual smFRET versus time trajectories for each PRE^{-A} complex. Contours are plotted from white (lowest population) to red (highest population). *n*, number of smFRET trajectories used to construct each contour plot. Corresponding one-dimensional FRET histograms plotted along right-hand *y*-axis of surface contour plots were generated using first 20 time points from all FRET trajectories in each data set. PRE^{-A} complexes without EF-G(GDPNP), top row; corresponding PRE^{-A} complexes with 2 μM EF-G(GDPNP), bottom row. (**a**) PRE$^{-A}_{fMet-1}$; (**b**) PRE$^{-A}_{fMet-2}$; (**c**) PRE$^{-A}_{Phe}$; (**d**) PRE$^{-A}_{Tyr}$; (**e**) PRE$^{-A}_{Glu}$; (**f**) PRE$^{-A}_{Val}$.

the aminoacyl acceptor stem of tRNA$^{fMet}_2$ to a Watson-Crick G-C base pair, the larger decrease in $k_{GS2\rightarrow GS1}$ (by almost an order of magnitude) relative to the smaller ~70% decrease of $k_{GS1\rightarrow GS2}$ drives the GS1↔GS2 equilibrium toward GS2 (**Table 1**). Biochemical and structural studies have shown that the aminoacyl acceptor stem of a P/P tRNA makes Watson-Crick base-pairing interactions with the P loop of 23S rRNA within the 50S subunit P site[30,31,34], whereas the aminoacyl acceptor stem of a P/E tRNA docks into a pocket formed by 23S rRNA helices H11, H68 and H74 within the 50S subunit E site, making a minor groove–minor groove interaction with H68 (refs. 32,33,35; **Fig. 6a**). Therefore, replacing the mismatched C1•A72 base pair with a Watson-Crick base pair could stabilize both of these interactions, but it would have a much larger effect on the minor groove–minor groove interaction between the aminoacyl acceptor stem of the tRNA and H68 (see Discussion).

Notably, our data suggest that the interactions of the tRNA aminoacyl acceptor stem with the P loop at the 50S subunit P site and H68 at the 50S E site are important regulators of $k_{GS1\rightarrow GS2}$ and $k_{GS2\rightarrow GS1}$, respectively. PRE complexes carrying a C1G A72C mutant tRNA^{fMet} analogous to tRNA^{Acc} have a faster rate of sparsomycin-promoted translocation relative to PRE complexes carrying P-site tRNA^{fMet} (ref. 10; sparsomycin is a ribosome-targeting antibiotic that promotes translocation through a mechanism that is closely related to that of EF-G-promoted translocation[36,37]). Considered alongside this translocation measurement, our results indicate that the greater stability of aminoacyl acceptor stem-H68 interactions in tRNAs carrying a Watson-Crick base pair at positions 1 and 72 is correlated with a greater rate of translocation (see **Supplementary Discussion**).

Altering the D stem or variable loop modulates $k_{GS1\rightarrow GS2}$

Similar to PRE$^{-A}_{Acc}$ complexes, PRE$^{-A}_{D\text{-}flip}$ complexes have a GS1↔GS2 equilibrium that is shifted toward GS2 relative to PRE$^{-A}_{fMet-2}$ complexes (**Figs. 2b**, **3b** and **5c** and **Table 1**). In contrast with PRE$^{-A}_{Acc}$ complexes, however, the shift toward GS2 in PRE$^{-A}_{D\text{-}flip}$ complexes primarily arises from about a three-fold increase in $k_{GS1\rightarrow GS2}$, with no substantial effect on $k_{GS2\rightarrow GS1}$ (**Table 1**). To further test the role of the A11-U24 base pair in modulating the GS1↔GS2 equilibrium, we generated an additional tRNA$^{fMet}_2$ A11C mutant, tRNA$^{D\text{-}dis}$, in which we introduced a mismatched C11•U24 base pair (**Fig. 4**, **Supplementary Methods** and **Supplementary Figs. 2**, **3** and **5**). Mirroring the results obtained with PRE$^{-A}_{D\text{-}flip}$, the GS1↔GS2 equilibrium in PRE$^{-A}_{D\text{-}dis}$ complexes was shifted toward GS2 relative to that in PRE$^{-A}_{fMet-2}$, and this effect arose from an ~1.8-fold increase in $k_{GS1\rightarrow GS2}$ and an almost negligible effect on $k_{GS2\rightarrow GS1}$ (**Figs. 2b**, **3b** and **5c**,**d** and **Table 1**).

Structural studies show that the D stem of the P/P tRNA makes a minor groove–minor groove interaction with 23S rRNA helix H69 within the 50S subunit P site; this interaction is completely disrupted when the tRNA is repositioned into the P/E configuration within GS2 (refs. 30–33; **Fig. 6a**). Although flipping or disrupting the purine-pyrimidine base pair between A11 and U24 could destabilize this minor groove–minor groove interaction, consequently destabilizing GS1 and increasing $k_{GS1\rightarrow GS2}$, X-ray structures of GS1-like ribosomal complexes show that the interactions between H69 and the D stem of a P/P tRNA^{fMet} or tRNA^{Phe} are almost indistinguishable[30,31]. Furthermore, deletion of H69 does not have a measurable effect on the yield or rate of translocation, suggesting that this interaction is not required for efficient translocation[38]. On the basis of these observations, we posit that the increase in $k_{GS1\rightarrow GS2}$ caused by the D stem mutations probably results from the effects that these mutations have on the structural stability of the tRNA itself, rather than from their potential effects on the interactions between the D stem and H69 (see Discussion).

Table 1 Equilibrium constants and transition rates governing the GS1↔GS2 equilibrium of PRE^{-A} complexes

P-site tRNA	Percent GS1[a]	Percent GS2[a]	K_{eq}[a]	$k_{GS1\rightarrow GS2}$ (s^{-1})[b]	$k_{GS2\rightarrow GS1}$ (s^{-1})[b]	Normalized $k_{GS1\rightarrow GS2}$[c]	Normalized $k_{GS2\rightarrow GS1}$[c]
				PRE^{-A}			
PRE$^{-A}_{fMet}$ complexes							
tRNA$^{fMet}_1$	79 ± 1	21 ± 1	0.27 ± 0.02	0.38 ± 0.12	1.30 ± 0.28	2.1 ± 0.9	1.0 ± 0.3
tRNA$^{fMet}_2$	**88 ± 2**	**12 ± 2**	**0.14 ± 0.02**	**0.18 ± 0.05**	**1.32 ± 0.33**	**1.0 ± 0.4**	**1.0 ± 0.3**
PRE$^{-A}_{elong}$ complexes							
tRNA^{Phe}	50 ± 6	50 ± 6	1.0 ± 0.2	0.50 ± 0.05	0.55 ± 0.08		
tRNA^{Tyr}	45 ± 4	55 ± 4	1.2 ± 0.2	0.56 ± 0.04	0.43 ± 0.06		
tRNA^{Glu}	61 ± 3	39 ± 3	0.64 ± 0.08	0.27 ± 0.05	0.59 ± 0.06		
tRNA^{Val}	63 ± 1	37 ± 1	0.58 ± 0.03	0.34 ± 0.08	0.69 ± 0.18		
PRE^{-A} complexes with tRNA^{fMet} mutants							
tRNA^{Anti}	89 ± 2	11 ± 2	0.12 ± 0.02	0.18 ± 0.04	1.48 ± 0.06	1.0 ± 0.4	1.1 ± 0.3
tRNA^{Acc}	73 ± 5	27 ± 5	0.38 ± 0.11	0.06 ± 0.03	0.15 ± 0.07	0.33 ± 0.18	0.12 ± 0.06
tRNA$^{D\text{-}flip}$	71 ± 2	29 ± 2	0.40 ± 0.04	0.60 ± 0.23	1.45 ± 0.30	3.4 ± 1.6	1.1 ± 0.4
tRNA$^{D\text{-}dis}$	75 ± 9	25 ± 9	0.35 ± 0.15	0.32 ± 0.10	1.53 ± 0.32	1.8 ± 0.8	1.2 ± 0.4
tRNA$^{Acc/D\text{-}flip}$	53 ± 2	47 ± 2	0.88 ± 0.09	0.11 ± 0.06	0.14 ± 0.07	0.61 ± 0.37	0.11 ± 0.06
				PRE^{-A} + 2 μM EF-G(GDPNP)[d]			
PRE$^{-A}_{fMet}$ complexes							
tRNA$^{fMet}_1$	33 ± 4	67 ± 4	2.1 ± 0.4	2.37 ± 0.36	0.87 ± 0.04		
tRNA$^{fMet}_2$	62 ± 5	38 ± 5	0.62 ± 0.14	0.52 ± 0.17	0.84 ± 0.22		
PRE^{-A} complexes with tRNA^{fMet} mutants							
tRNA^{Anti}	60 ± 1	40 ± 1	0.67 ± 0.03	0.46 ± 0.22	0.73 ± 0.23		
tRNA^{Acc}	30 ± 8	70 ± 8	2.4 ± 0.9	0.23 ± 0.10	0.03 ± 0.10		
tRNA$^{D\text{-}flip}$	26 ± 5	74 ± 5	2.9 ± 0.9	1.95 ± 0.20	0.58 ± 0.23		
tRNA$^{D\text{-}dis}$	30 ± 2	70 ± 2	2.4 ± 0.2	2.17 ± 0.14	1.09 ± 0.09		

Mean ± s.d. of equilibrium constant and transition rates for each PRE^{-A} complex were calculated from three independent data sets.
[a]Fractional populations of GS1 and GS2 and equilibrium constants were calculated as described in **Supplementary Methods**. [b]Transition rates were calculated using dwell-time analysis and corrected for fluorophore photobleaching (see Online Methods and **Supplementary Methods**). [c]Transition rates for PRE^{-A} complexes carrying tRNA$^{fMet}_1$ or tRNA$^{fMet}_2$ mutants are normalized to PRE$^{-A}_{fMet\text{-}2}$ (shown in bold) for comparison. [d]Transition rates were not calculated for PRE^{-A} complexes with smFRET trajectories that primarily or exclusively occupy SP_{GS2} in the presence of EF-G(GDPNP) (**Fig. 2** and **Supplementary Table 1**).

Further evidence that perturbations to the structural stability of the P-site tRNA might modulate the GS1↔GS2 equilibrium comes from a comparison of PRE$^{-A}_{fMet\text{-}1}$ and PRE$^{-A}_{fMet\text{-}2}$ complexes (**Fig. 3a**,**b**). Similar to PRE$^{-A}_{D\text{-}flip}$ and PRE$^{-A}_{D\text{-}dis}$ complexes, PRE$^{-A}_{fMet\text{-}1}$ complexes have a GS1↔GS2 equilibrium shifted toward GS2 relative to that in PRE$^{-A}_{fMet\text{-}2}$ complexes, through a kinetic mechanism involving about a two-fold increase in $k_{GS1\rightarrow GS2}$ and no detectable change in $k_{GS2\rightarrow GS1}$ (**Table 1**). The only difference between tRNA$^{fMet}_1$ and tRNA$^{fMet}_2$ is a change at nucleotide 46 within the variable loop from a 7-methylguanosine (^{7}mG) in tRNA$^{fMet}_1$ to an adenosine in tRNA$^{fMet}_2$ (refs. 24,27). In this case, however, structures of GS1- and GS2-like ribosomal complexes show that the variable loop of tRNA^{fMet} does not directly contact the ribosome when tRNA^{fMet} is in either the P/P or P/E configuration[31,32], suggesting that slight differences in the structural stability of P site–bound tRNA$^{fMet}_1$ versus tRNA$^{fMet}_2$ are responsible for the observed increase in $k_{GS1\rightarrow GS2}$. The notion that the relatively subtle differences in the sequences within the D stems and variable loops of tRNA$^{fMet}_2$, tRNA$^{D\text{-}flip}$, tRNA$^{D\text{-}dis}$ and tRNA$^{fMet}_1$ lead to differences in the structural stabilities of these tRNAs is supported by their distinct migrations on a native polyacrylamide gel (**Supplementary Fig. 2** and **Supplementary Discussion**).

tRNA^{fMet} double mutant has elongator-like behavior

Despite their ability to shift the GS1↔GS2 equilibrium toward GS2, both PRE$^{-A}_{Acc}$ and PRE$^{-A}_{D\text{-}flip}$ complexes rapidly fluctuated between GS1 and GS2 in the presence of EF-G(GDPNP), similarly to PRE$^{-A}_{fMet}$ complexes (**Figs. 3a**,**b** and **5b**,**c** and **Table 1**). This suggests that neither replacing the C1•A72 mismatched base pair with a Watson-Crick base pair within the aminoacyl acceptor stem nor flipping the purine-pyrimidine base pair between A11 and U24 to a pyrimidine-purine base pair within the D stem of tRNA^{fMet} enables EF-G to modulate

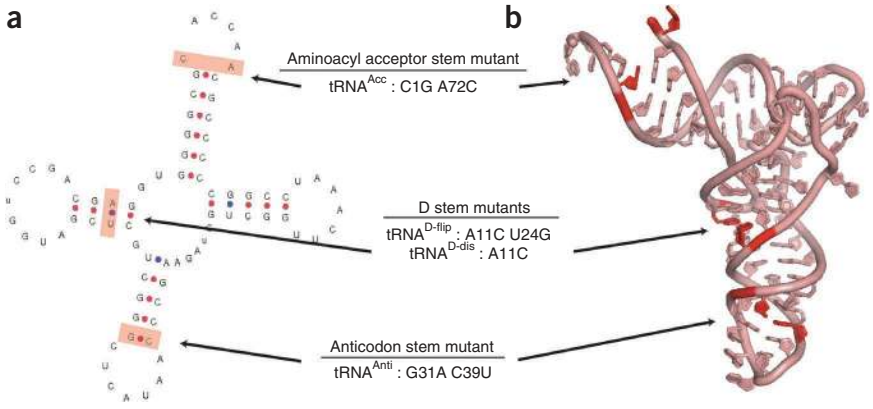

Figure 4 Design of tRNA$^{fMet}_2$ mutants. (**a**) Secondary structure diagram for *E. coli* tRNA$^{fMet}_2$. Three structural features of tRNA^{fMet} differentiating it from all elongator tRNAs, red; mutations designed to convert these three structural features to those found in tRNA^{Phe} are listed. (**b**) Three-dimensional structure of *E. coli* tRNA$^{fMet}_2$. Three unique structural features of tRNA^{fMet} are colored as in the secondary structure diagram[44] (PDB 3CW6).

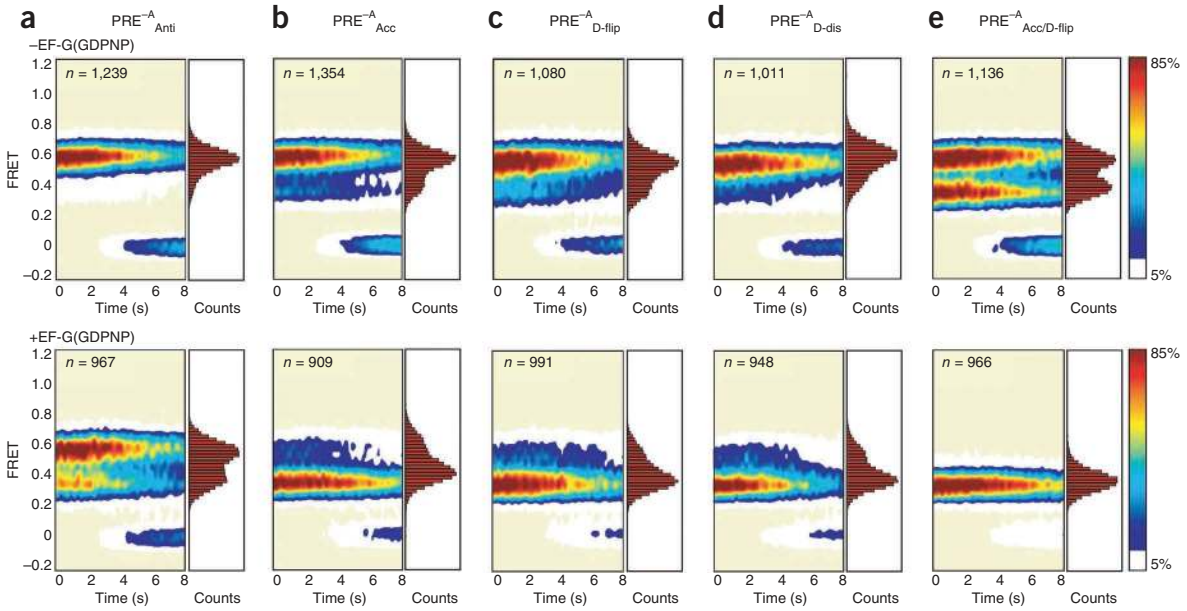

Figure 5 Steady-state smFRET measurements on PRE^{-A} complexes carrying tRNA$^{fMet}_2$ mutants. Data are presented as in **Figure 3**. (**a**) PRE$^{-A}_{Anti}$; (**b**) PRE$^{-A}_{Acc}$; (**c**) PRE$^{-A}_{D\text{-}flip}$; (**d**) PRE$^{-A}_{D\text{-}dis}$; (**e**) PRE$^{-A}_{Acc/D\text{-}flip}$.

the GS1↔GS2 equilibrium of the corresponding PRE complexes in the same manner as it does in the PRE$^{-A}_{elong}$ complexes we examined. This prompted us to design a tRNA$^{fMet}_2$ double mutant combining the aminoacyl acceptor stem and D stem mutations (tRNA$^{Acc/D\text{-}flip}$; **Supplementary Figs. 2** and **5**). We found that PRE$^{-A}_{Acc/D\text{-}flip}$ complexes had kinetic effects on the GS1↔GS2 equilibrium that were roughly the sum of those observed for PRE$^{-A}_{Acc}$ and PRE$^{-A}_{D\text{-}flip}$ complexes. Before the addition of EF-G(GDPNP), the double mutation led to a large, approximately six-fold shift in the K_{eq} governing the GS1↔GS2 equilibrium toward GS2, which was predominantly driven by a decrease in $k_{GS2\rightarrow GS1}$ by an order of magnitude and a slight, ~40% decrease in $k_{GS1\rightarrow GS2}$ relative to the corresponding parameters for the PRE$^{-A}_{fMet\text{-}2}$ complex (**Figs. 3b** and **5e** and **Table 1**). Notably, although K_{eq} for the PRE$^{-A}_{Acc/D\text{-}flip}$ complex was within the range of K_{eq} values for the PRE$^{-A}_{elong}$ complexes, $k_{GS1\rightarrow GS2}$ and $k_{GS2\rightarrow GS1}$ for the PRE$^{-A}_{Acc/D\text{-}flip}$ complex were both ~50–80% slower than those for the PRE$^{-A}_{elong}$ complexes investigated in this study. This indicates that although we have uncovered two structural elements of tRNA^{fMet} that influence its GS1↔GS2 dynamics, additional, unidentified structural features of tRNA^{fMet} probably also participate in this regulation. Nevertheless, in contrast to the PRE$^{-A}_{Acc}$ and PRE$^{-A}_{D\text{-}flip}$ complexes, the PRE$^{-A}_{Acc/D\text{-}flip}$ complex is highly stabilized in GS2 in the presence of EF-G(GDPNP), with thermodynamic and kinetic behavior indistinguishable from that of the PRE$^{-A}_{elong}$ complexes we examined (**Figs. 2b**, **3** and **5e**). This result suggests that the structural stability of the P-site tRNA and the interactions this tRNA makes with the ribosome can effectively regulate the ability of EF-G to stabilize GS2. Consequently, it suggests that these features may affect how efficiently EF-G catalyzes translocation.

DISCUSSION

Interactions of P/E tRNA with H68 affect stability of GS2

Our results demonstrate that PRE$^{-A}_{fMet}$ complexes have GS1↔GS2 dynamics with and without EF-G(GDPNP) that differ substantially from those observed in PRE$^{-A}_{elong}$ complexes. Notably, our findings show how specific tRNA-ribosome interactions and tRNA structural features modulate $k_{GS1\rightarrow GS2}$ and $k_{GS2\rightarrow GS1}$ to drive these differences. The effects of altering individual tRNA^{fMet} structural features on PRE^{-A} complex dynamics can be interpreted in terms of the ability of each alteration to stabilize or destabilize GS1 and/or GS2. In this regard, structural interpretations based on the available X-ray and cryo-EM structures of GS1- and GS2-like ribosomes[30–33] are especially enlightening.

The largest effect we observed was a decrease in $k_{GS2\rightarrow GS1}$ by an order of magnitude caused by replacing the mismatched C1•A72 base pair with a Watson-Crick base pair within the aminoacyl acceptor stem of tRNA^{fMet}. We speculate that introducing this Watson-Crick base pair stabilizes GS2 by stabilizing the minor groove–minor groove interaction between H68 and nucleotides 70 and 71 in the tRNA aminoacyl acceptor stem[30–33,35]. Such an interpretation suggests that this minor groove–minor groove interaction is sensitive to the detailed helical geometry of the aminoacyl acceptor stem. Highlighting the functional importance of this interaction, biochemical studies have shown that PRE complexes carrying a P-site tRNA in which the 2′-hydroxyl at nucleotide 71 has been modified to disrupt its minor groove–minor groove interaction with H68 have a ≥90% reduced rate of EF-G-promoted translocation[39]. In addition to this minor groove–minor groove interaction, a recent molecular dynamics simulation comparing the interactions of H68 with the aminoacyl acceptor stem of either P/E tRNA^{fMet} or tRNA^{Phe} suggests that the universally conserved 23S rRNA U1851•G1891 wobble base pair within H68 can be disrupted such that U1851 can flip out of H68 and establish a wobble base-pairing interaction with G70 of tRNA^{Phe}. Notably, this interaction is not observed in an analogous simulation using a P/E tRNA^{fMet}, providing an additional rationale for the enhanced ability of tRNA^{Phe} to stabilize GS2 relative to that of tRNA^{fMet} (ref. 40).

Flexibility of P/P tRNA modulates stability of GS1

tRNA$^{D\text{-}flip}$, tRNA$^{D\text{-}dis}$ and tRNA$^{fMet}_1$ differ from tRNA$^{fMet}_2$ at a single base pair within the D stem (tRNA$^{D\text{-}flip}$ and tRNA$^{D\text{-}dis}$) or at a single nucleotide within the variable loop (tRNA$^{fMet}_1$). As discussed in Results, the effect of these differences on $k_{GS1\rightarrow GS2}$ for the corresponding PRE^{-A} complexes probably originates from differences in

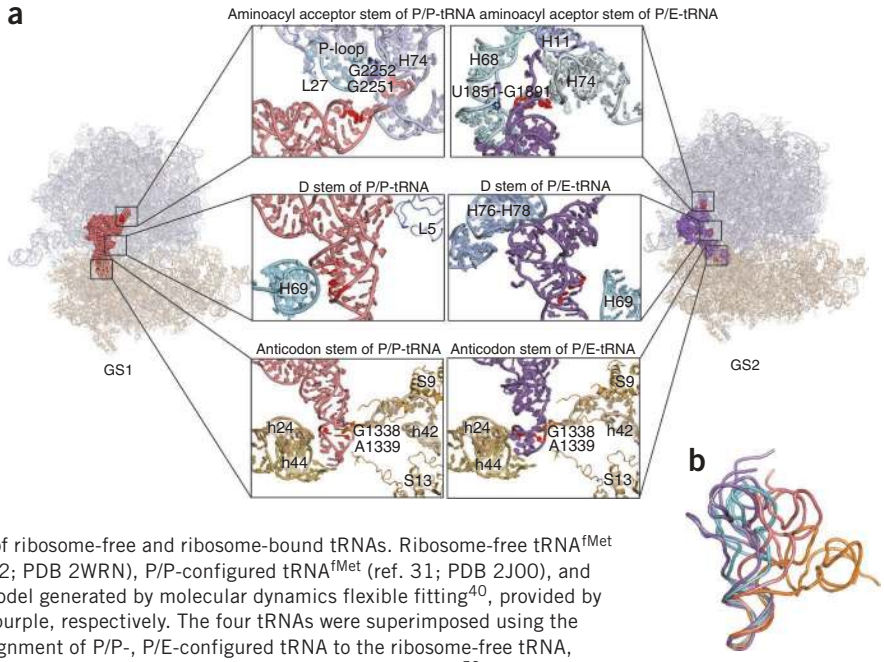

Figure 6 P-site tRNA-ribosome interactions within the GS1 and GS2 state of a PRE complex and comparative structural analysis of ribosome-free and ribosome-bound tRNAs. (**a**) P-site tRNA-ribosome interactions within GS1 and GS2 state of a PRE complex. Quasi-atomic-resolution models for GS1 (left) and GS2 (right) states of a PRE complex were generated by real-space refinement using rigid body fitting of atomic-resolution structures of the *E. coli* ribosome (PDB 2AVY and 2AW4) and a P site–bound tRNA (PDB 2J00) into the electron density obtained from cryo-EM reconstructions of the GS1 and GS2 states of a PRE complex (provided by J. Frank, H. Gao and X. Aguirrezabala)[32]. P/P- and P/E-configured tRNAs, pink and purple, respectively. rRNA helices and r-proteins that interact with aminoacyl acceptor stem (top), D stem (middle) and anticodon stem (bottom) of each tRNA are labeled; nucleotide positions of $tRNA^{fMet}_2$ mutations, red. (**b**) Comparative structural analysis of ribosome-free and ribosome-bound tRNAs. Ribosome-free $tRNA^{fMet}$ (ref. 44; PDB 3CW6), A/T-configured $tRNA^{Thr}$ (ref. 22; PDB 2WRN), P/P-configured $tRNA^{fMet}$ (ref. 31; PDB 2J00), and P/E-configured $tRNA^{fMet}$ (quasi-atomic-resolution model generated by molecular dynamics flexible fitting[40], provided by K. Schulten and B. Liu) are cyan, orange, pink and purple, respectively. The four tRNAs were superimposed using the anticodon stem loops (nucleotides 31–39 for the alignment of P/P-, P/E-configured tRNA to the ribosome-free tRNA, and nucleotides 32–38 for the alignment of A/T-configured tRNA to the ribosome-free tRNA) with PyMol[50].

the structural stabilities of the tRNAs themselves. The characteristic L-shaped tertiary structure of tRNA is determined and stabilized by coaxial stacking of the aminoacyl acceptor and T stems, coaxial stacking of the D and anticodon stems, and a network of base-pairing and base-stacking interactions among the T, D and variable loops[41]. The delicate network of tertiary interactions that stabilizes its the L-shaped structure has been noted since the earliest structural studies of tRNA, as has the possible functional importance of its structurally determined, intrinsic conformational flexibility during protein synthesis[41,42].

A well-studied mechanistic step during translation featuring the conformational flexibility of tRNA is the elongation factor Tu (EF-Tu)-catalyzed aa-tRNA selection step of the elongation cycle. During this process, the aa-tRNA adopts a functionally critical intermediate conformation, termed the A/T configuration, which requires a marked distortion of the aa-tRNA centered at the junction between the anticodon and D stems[21–23] (**Fig. 6b**). Similarly, P/P tRNAs have a pronounced distortion centered at the same junction[2,21,22,30,31]. More specifically, the D stem of the P/P tRNA is partially unwound relative to its anticodon stem, and the tRNA is kinked at a hinge formed by the G26-A44 base pair at the junction between the anticodon and D stems so that it is positioned toward the 50S subunit and slightly toward the A site[2,30,31] (**Fig. 6b**). Therefore, the stability of the distorted conformation adopted by a particular P/P tRNA could contribute substantially to the stability of GS1 and, consequently, to the $k_{GS1 \rightarrow GS2}$ of the corresponding PRE^{-A} complex.

Viewed through this lens, the specific interactions that define and stabilize the tertiary structure of a particular tRNA would govern its conformational flexibility and influence the stability of the distorted conformation it adopts within the P/P configuration. For example, the identity of nucleotide 46 in $tRNA^{fMet}$ (^{7}mG46 in $tRNA^{fMet}_1$ and A46 in $tRNA^{fMet}_2$) might affect the conformational flexibility of $tRNA^{fMet}$ via the highly conserved base-triple interaction between nucleotide 46 and the C13-G22 base pair within the D stem of $tRNA^{fMet}$ (refs. 41,43,44). Notably, whereas this base triple is observed in ribosome-free $tRNA^{fMet}$ (refs. 41,43,44), it is apparently disrupted when $tRNA^{fMet}$ adopts the distorted P/P configuration[30,31]. Because the A46•C13-G22 base triple is weaker than the ^{7}mG46•C13-G22 base triple[43–45], disrupting this tertiary interaction in $tRNA^{fMet}_2$ is probably less energetically costly than disrupting it in $tRNA^{fMet}_1$. Thus, we expect $tRNA^{fMet}_2$ to be energetically more stable than $tRNA^{fMet}_1$ when it adopts the distorted P/P configuration within GS1, providing a molecular basis for the observed higher stability of GS1 in PRE^{-A}_{fMet-2}, and hence its slower $k_{GS1 \rightarrow GS2}$, relative to PRE^{-A}_{fMet-1}. Likewise, perturbations to the D stem of $tRNA^{fMet}$ (as in $tRNA^{D-flip}$ and $tRNA^{D-dis}$) might alter the conformational flexibility of the tRNA by directly affecting the structural integrity of the D stem. Nevertheless, it is difficult to predict the effect of particular sequence alteration on the conformational flexibility of a tRNA solely on the basis of the X-ray crystal structure of that tRNA; this is primarily because it is difficult to assess the conformational entropy of a biomolecule using its X-ray crystal structure[46]. For example, the observation that weakening the A11-U24 base pair via the A11C mutation in $tRNA^{D-dis}$ has a smaller effect on $k_{GS1 \rightarrow GS2}$ than strengthening it via the A11C U24G mutations in $tRNA^{D-flip}$ suggests a complex interplay among the tertiary structure and conformational flexibility of a particular tRNA and the stability of its corresponding PRE^{-A} complex in GS1; additional X-ray structures, smFRET studies and computational simulations will probably be necessary for researchers to fully understand this interplay.

In addition to its role in modulating the stability of GS1, the intrinsic conformational flexibility of the tRNA could directly influence the transition from its P/P to its P/E configuration (see **Supplementary Discussion**). Regardless, on the basis of our data and this discussion, we predict that variations in the structure of tRNA within or near the junction between the anticodon and D stems would influence $k_{GS1 \rightarrow GS2}$. Future smFRET experiments to evaluate the effect of systematic mutations within this region of a single tRNA species should allow testing of this hypothesis and a more thorough mapping of the relationship between the stability of this junction and $k_{GS1 \rightarrow GS2}$.

As we were completing this article, we became aware of an X-ray crystal structure of a GS2-like ribosomal complex carrying a full-length deacylated P/E $tRNA^{Phe}$ (ref. 47). This new X-ray crystal structure provides views at near-atomic resolution of the ribosome-tRNA

interactions and tRNA distortion originally identified at lower resolution through cryo-EM studies of GS2-like PRE complexes[32,33] and confirms the structural interpretations reported above.

tRNA-mediated PRE complex dynamics may regulate elongation

Collectively, our results demonstrate that the P-site tRNA is a key regulator of PRE complex dynamics. Notably, each PRE^{-A} complex we investigated has unique GS1↔GS2 dynamics (**Table 1**). On the basis of the discussion above, we expect that the particular structural features of each tRNA species differentially regulate the GS1↔GS2 equilibrium. Taking into consideration this point together with data suggesting that the GS1→GS2 transition may be rate limiting for EF-G–promoted translocation[6,12] and that PRE complexes that preferentially occupy GS2 are more efficiently translocated by EF-G[10,20], it is possible that incorporation of specific tRNAs at particular codons of an mRNA is used to regulate the rate of translation elongation at those codons. In this view, tRNA-mediated control of the GS1↔GS2 equilibrium could allow selective attenuation of EF-G–promoted translocation and serve as a point of translational regulation (see **Supplementary Discussion**). Consistent with this possibility, the observed lower occupancy of GS2 in PRE_{fMet} complexes relative to PRE_{elong} complexes provides a mechanistic rationale for the recent observation that EF-G–promoted translocation of the PRE_{fMet} complex during the first round of translation elongation is slower than EF-G–promoted translocation during subsequent rounds of translation elongation[48,49].

Distinct dynamics may reflect unique selective pressures

On the basis of our data, we hypothesize that the dynamics of PRE_{fMet} complexes relative to the PRE_{elong} complexes we studied may arise from the different biochemical functions of $tRNA^{fMet}$ and elongator tRNAs and the distinct selective pressures under which these two types of tRNAs have evolved. The presence of a Watson-Crick or wobble base pair versus a mismatched base pair between nucleotides 1 and 72 of the aminoacyl acceptor stem is the primary feature by which EF-Tu discriminates elongator tRNAs from $tRNA^{fMet}$ during translation elongation[27]. Our results demonstrate that this sequence and structural feature primarily modulates the stability of GS2. In addition, elongator tRNAs undergo distortions at the junction between the anticodon and D stems as the incoming aa-tRNA passes through the A/T configuration during aa-tRNA selection, and as the newly formed peptidyl tRNA is positioned into the P/P configuration after translocation from the A site into the P site. Thus, the conformational flexibility of each elongator tRNA has probably been optimized for, among other things, high-fidelity aa-tRNA selection and translocation of peptidyl tRNA from the A site to the P site. In contrast, $tRNA^{fMet}$ does not undergo aa-tRNA selection into the A site, nor is it loaded into the P site through a translocation event from the A site. Instead, $tRNA^{fMet}$, with only a single amino acid attached to its aminoacyl acceptor end, binds directly to the P site of the 30S subunit as part of the formation of the 30S initiation complex and adopts the P/P configuration as the 50S subunit joins to the 30S initiation complex during translation initiation[27]. Thus, in contrast to elongator tRNAs, $tRNA^{fMet}$ has an intrinsic conformational flexibility that has been optimized for proper positioning within the 30S initiation complex, participation in the mechanism of 50S subunit joining and maintenance of the P/P configuration even without a bona fide polypeptide at its aminoacyl acceptor end. The selective pressures under which $tRNA^{fMet}$ has evolved relative to elongator tRNAs have generated unique sequence and structural elements in $tRNA^{fMet}$ leading to the properties of GS1↔GS2 dynamics and translocation observed in ribosomal complexes carrying this P-site tRNA.

METHODS

Methods and any associated references are available in the online version of the paper at http://www.nature.com/nsmb/.

Note: Supplementary information is available on the Nature Structural & Molecular Biology website.

ACKNOWLEDGMENTS

We thank U. RajBhandary for providing us with the plasmids and strains necessary to generate, overexpress and purify all $tRNA^{fMet}$ mutants reported here; J. Frank, H. Gao and X. Aguirrezabala for providing us with structural models for GS1 and GS2; K. Schulten and B. Liu for providing us with a quasi-atomic-resolution model of a hybrid P/E–configured tRNA; J. Cate for providing us with an early preprint of ref. 47; D. MacDougall, W. Ning, S. Mitra, C. Perez and J. Cate for valuable discussions and comments on the manuscript; and C. Perez for managing the Gonzalez laboratory. This work was supported by grants to R.L.G. from the Burroughs Wellcome Fund (CABS 1004856), the US National Science Foundation (MCB 0644262) and the US National Institute of General Medical Sciences (GM 084288). A.C.R. was supported, in part, by the Amgen Scholars Program at Columbia University.

AUTHOR CONTRIBUTIONS

J.F. and R.L.G. Jr. designed the research; J.F. and A.C.R. carried out the experiments and analyzed the data; J.E.B. helped with the data analysis; J.F., A.C.R. and R.L.G. Jr. wrote the manuscript; all authors approved the final manuscript.

COMPETING FINANCIAL INTERESTS

The authors declare no competing financial interests.

Published online at http://www.nature.com/nsmb/.
Reprints and permissions information is available online at http://www.nature.com/reprints/index.html.

1. Frank, J., Gao, H., Sengupta, J., Gao, N. & Taylor, D.J. The process of mRNA-tRNA translocation. *Proc. Natl. Acad. Sci. USA* **104**, 19671–19678 (2007).
2. Korostelev, A. & Noller, H.F. The ribosome in focus: new structures bring new insights. *Trends Biochem. Sci.* **32**, 434–441 (2007).
3. Shoji, S., Walker, S.E. & Fredrick, K. Ribosomal translocation: one step closer to the molecular mechanism. *ACS Chem. Biol.* **4**, 93–107 (2009).
4. Blanchard, S.C., Kim, H.D., Gonzalez, R.L. Jr., Puglisi, J.D. & Chu, S. tRNA dynamics on the ribosome during translation. *Proc. Natl. Acad. Sci. USA* **101**, 12893–12898 (2004).
5. Frank, J. & Gonzalez, R.L. Jr. Structure and dynamics of a processive brownian motor: the translating ribosome. *Annu. Rev. Biochem.* **79**, 381–412 (2010).
6. Fei, J., Kosuri, P., MacDougall, D.D. & Gonzalez, R.L. Jr. Coupling of ribosomal L1 stalk and tRNA dynamics during translation elongation. *Mol. Cell* **30**, 348–359 (2008).
7. Fei, J. Allosteric collaboration between elongation factor G and the ribosomal L1 stalk directs tRNA movements during translation. *Proc. Natl. Acad. Sci. USA* **106**, 15702–15707 (2009).
8. Cornish, P.V., Ermolenko, D.N., Noller, H.F. & Ha, T. Spontaneous intersubunit rotation in single ribosomes. *Mol. Cell* **30**, 578–588 (2008).
9. Cornish, P.V. *et al.* Following movement of the L1 stalk between three functional states in single ribosomes. *Proc. Natl. Acad. Sci. USA* **106**, 2571–2576 (2009).
10. Dorner, S., Brunelle, J.L., Sharma, D. & Green, R. The hybrid state of tRNA binding is an authentic translation elongation intermediate. *Nat. Struct. Mol. Biol.* **13**, 234–241 (2006).
11. Munro, J.B., Altman, R.B., Tung, C.S., Sanbonmatsu, K.Y. & Blanchard, S.C. A fast dynamic mode of the EF-G-bound ribosome. *EMBO J.* **29**, 770–781 (2010).
12. Munro, J.B., Wasserman, M.R., Altman, R.B., Wang, L. & Blanchard, S.C. Correlated conformational events in EF-G and the ribosome regulate translocation. *Nat. Struct. Mol. Biol.* **17**, 1470–1477 (2010).
13. Moazed, D. & Noller, H.F. Intermediate states in the movement of transfer RNA in the ribosome. *Nature* **342**, 142–148 (1989).
14. Ermolenko, D.N. *et al.* Observation of intersubunit movement of the ribosome in solution using FRET. *J. Mol. Biol.* **370**, 530–540 (2007).
15. Munro, J.B. *et al.* Spontaneous formation of the unlocked state of the ribosome is a multistep process. *Proc. Natl. Acad. Sci. USA* **107**, 709–714 (2010).
16. Zavialov, A.V. & Ehrenberg, M. Peptidyl-tRNA regulates the GTPase activity of translation factors. *Cell* **114**, 113–122 (2003).
17. Modolell, J., Cabrer, B. & Vaquez, D. The interaction of elongation factor G with N-acetylphenylalanyl transfer RNA-ribosome complexes. *Proc. Natl. Acad. Sci. USA* **70**, 3561–3565 (1973).
18. Connell, S.R. *et al.* Structural basis for interaction of the ribosome with the switch regions of GTP-bound elongation factors. *Mol. Cell* **25**, 751–764 (2007).
19. Valle, M. *et al.* Locking and unlocking of ribosomal motions. *Cell* **114**, 123–134 (2003).

20. Studer, S.M., Feinberg, J.S. & Joseph, S. Rapid kinetic analysis of EF-G-dependent mRNA translocation in the ribosome. *J. Mol. Biol.* **327**, 369–381 (2003).
21. Villa, E. *et al.* Ribosome-induced changes in elongation factor Tu conformation control GTP hydrolysis. *Proc. Natl. Acad. Sci. USA* **106**, 1063–1068 (2009).
22. Schmeing, T.M. *et al.* The crystal structure of the ribosome bound to EF-Tu and aminoacyl-tRNA. *Science* **326**, 688–694 (2009).
23. Voorhees, R.M., Schmeing, T.M., Kelley, A.C. & Ramakrishnan, V. The mechanism for activation of GTP hydrolysis on the ribosome. *Science* **330**, 835–838 (2010).
24. Ishii, S., Kuroki, K. & Imamoto, F. tRNAMetf2 gene in the leader region of the nusA operon in *Escherichia coli*. *Proc. Natl. Acad. Sci. USA* **81**, 409–413 (1984).
25. Varshney, U., Lee, C.P. & RajBhandary, U.L. From elongator tRNA to initiator tRNA. *Proc. Natl. Acad. Sci. USA* **90**, 2305–2309 (1993).
26. RajBhandary, U.L. Initiator transfer RNAs. *J. Bacteriol.* **176**, 547–552 (1994).
27. Laursen, B.S., Sorensen, H.P., Mortensen, K.K. & Sperling-Petersen, H.U. Initiation of protein synthesis in bacteria. *Microbiol. Mol. Biol. Rev.* **69**, 101–123 (2005).
28. Mayer, C., Stortchevoi, A., Kohrer, C., Varshney, U. & RajBhandary, U.L. Initiator tRNA and its role in initiation of protein synthesis. *Cold Spring Harb. Symp. Quant. Biol.* **66**, 195–206 (2001).
29. Kolitz, S.E. & Lorsch, J.R. Eukaryotic initiator tRNA: finely tuned and ready for action. *FEBS Lett.* **584**, 396–404 (2010).
30. Korostelev, A., Trakhanov, S., Laurberg, M. & Noller, H.F. Crystal structure of a 70S ribosome-tRNA complex reveals functional interactions and rearrangements. *Cell* **126**, 1065–1077 (2006).
31. Selmer, M. *et al.* Structure of the 70S ribosome complexed with mRNA and tRNA. *Science* **313**, 1935–1942 (2006).
32. Agirrezabala, X. *et al.* Visualization of the hybrid state of tRNA binding promoted by spontaneous ratcheting of the ribosome. *Mol. Cell* **32**, 190–197 (2008).
33. Julián, P. *et al.* Structure of ratcheted ribosomes with tRNAs in hybrid states. *Proc. Natl. Acad. Sci. USA* **105**, 16924–16927 (2008).
34. Samaha, R.R., Green, R. & Noller, H.F. A base pair between tRNA and 23S rRNA in the peptidyl transferase centre of the ribosome. *Nature* **377**, 309–314 (1995).
35. Yusupov, M.M. *et al.* Crystal structure of the ribosome at 5.5 Å resolution. *Science* **292**, 883–896 (2001).
36. Fredrick, K. & Noller, H.F. Catalysis of ribosomal translocation by sparsomycin. *Science* **300**, 1159–1162 (2003).
37. Southworth, D.R. & Green, R. Ribosomal translocation: sparsomycin pushes the button. *Curr. Biol.* **13**, R652–R654 (2003).
38. Ali, I.K., Lancaster, L., Feinberg, J., Joseph, S. & Noller, H.F. Deletion of a conserved, central ribosomal intersubunit RNA bridge. *Mol. Cell* **23**, 865–874 (2006).
39. Feinberg, J.S. & Joseph, S. Identification of molecular interactions between P-site tRNA and the ribosome essential for translocation. *Proc. Natl. Acad. Sci. USA* **98**, 11120–11125 (2001).
40. Trabuco, L.G. *et al.* The role of L1 stalk-tRNA interaction in the ribosome elongation cycle. *J. Mol. Biol.* **402**, 741–760 (2010).
41. Rich, A. & RajBhandary, U.L. Transfer RNA: molecular structure, sequence, and properties. *Annu. Rev. Biochem.* **45**, 805–860 (1976).
42. Alexander, R.W., Eargle, J. & Luthey-Schulten, Z. Experimental and computational determination of tRNA dynamics. *FEBS Lett.* **584**, 376–386 (2010).
43. Daniel, W.E. Jr. & Cohn, M. Changes in tertiary structure accompanying a single base change in transfer RNA. Proton magnetic resonance and aminoacylation studies of *Escherichia coli* tRNAMet f1 and tRNAMet f3 and their spin-labeled (s4U8) derivatives. *Biochemistry* **15**, 3917–3924 (1976).
44. Barraud, P., Schmitt, E., Mechulam, Y., Dardel, F. & Tisne, C. A unique conformation of the anticodon stem-loop is associated with the capacity of tRNAfMet to initiate protein synthesis. *Nucleic Acids Res.* **36**, 4894–4901 (2008).
45. Mandal, N. & RajBhandary, U.L. *Escherichia coli* B lacks one of the two initiator tRNA species present in *E. coli* K-12. *J. Bacteriol.* **174**, 7827–7830 (1992).
46. Uhlenbeck, O.C. RNA biophysics has come of age. *Biopolymers* **91**, 811–814 (2009).
47. Dunkle, J.A. *et al.* Structures of the bacterial ribosome in classical and hybrid states of tRNA binding. *Science* **332**, 981–984 (2011).
48. Uemura, S. *et al.* Real-time tRNA transit on single translating ribosomes at codon resolution. *Nature* **464**, 1012–1017 (2010).
49. Aitken, C.E. & Puglisi, J.D. Following the intersubunit conformation of the ribosome during translation in real time. *Nat. Struct. Mol. Biol.* **17**, 793–800 (2010).
50. Schrodinger, LLC. The PyMOL Molecular Graphics System, Version 1.3r1. (2010).

ONLINE METHODS

mRNA preparation. All mRNAs used were derived from a described variant of an mRNA encoding the first 20 amino acids of gene product 32 from T4 bacteriophage[51]. Five mRNAs were designed so that their first codons coded for fMet (AUG), phenylalanine (UUC), tyrosine (UAC), glutamate (GAA) or valine (GUU). All five mRNAs were otherwise identical and contained no other codons coding for the anticodons of $tRNA^{fMet}$, $tRNA^{Phe}$, $tRNA^{Tyr}$, $tRNA^{Glu}$ or $tRNA^{Val}$ in any reading frame (**Supplementary Fig. 1**). All mRNAs were *in vitro*–transcribed from linearized plasmid DNA templates using T7 RNA polymerase according to a described protocol[52–55]. A 3′-biotinylated DNA oligonucleotide (TGTGTAAGTTTTAGGTTGATTTG-biotin; Integrated DNA Technologies) complementary to the 5′ end of the mRNAs was then hybridized to these mRNAs to enable surface immobilization as described[54,55]. We refer to mRNA transcripts hybridized to a 3′-biotinylated DNA oligonucleotide are as biotin-mRNAs.

tRNA mutagenesis and purification. The pUC13.trnfM plasmid (a gift from U. RajBhandary, Massachusetts Institute of Technology, Cambridge, Massachusetts, USA) carrying the *E. coli metY* gene, which encodes $tRNA^{fMet}$ isoacceptor 2, $tRNA^{fMet}_2$ (ref. 24), was mutated to generate $tRNA^{fMet}_1$ and all $tRNA^{fMet}_2$ mutants. $tRNA^{fMet}_2$ mutants included $tRNA^{Anti}$ (G31A C39U), in which the G31-C39 base pair in the anticodon stem of $tRNA^{fMet}_2$ was changed to the A31-U39 base pair found in $tRNA^{Phe}$; $tRNA^{Acc}$ (C1G A72C), in which the mismatched C1•A72 base pair in the aminoacyl acceptor stem of $tRNA^{fMet}_2$ was changed to the G1-C72 Watson-Crick base pair found in $tRNA^{Phe}$; $tRNA^{D\text{-}flip}$ (A11C U24G), in which the purine-pyrimidine A11-U24 base pair within the D stem of $tRNA^{fMet}_2$ was flipped to the pyrimidine-purine C11-G24 base pair found in $tRNA^{Phe}$; $tRNA^{D\text{-}dis}$ (A11C), in which the A11-U24 base pair within the D stem was disrupted by changing A11 to C11; and $tRNA^{Acc/D\text{-}flip}$ (C1G A11C U24G A72C), in which the mutations generated in $tRNA^{Acc}$ and $tRNA^{D\text{-}flip}$ were combined. All tRNAs were expressed in *E. coli* strain B105, which lacks the *metY* gene and therefore endogenous $tRNA^{fMet}_2$, and were purified using a described protocol[45,56,57] with slight modifications. Briefly, $tRNA^{fMet}_1$ and $tRNA^{fMet}_2$ (or $tRNA^{fMet}_2$ mutants) were separated from each other, from elongator tRNAs and from all other cellular RNA species by native PAGE on a 15% (w/v) gel (**Supplementary Fig. 2**). tRNA bands were identified by UV shadowing at a wavelength of 254 nm, cut from the gel and eluted from the gel slices using RNA Elution Buffer (10 mM Tris hydrochloride, $pH_{25\,°C}$ 7.5, 1 mM ethylenediamine tetraacetic acid and 10 mM sodium chloride). The PAGE-purified tRNAs were further purified on a Phenyl 5PW TSK-Gel hydrophobic interaction chromatography (HIC) column (Tosoh Bioscience) using a gradient from HIC Buffer A (1.7 M ammonium sulfate and 10 mM ammonium acetate, pH 6.3) to HIC Buffer B (10% (v/v) methanol and 10 mM ammonium acetate, pH 6.3; **Supplementary Fig. 3**).

Assembly and purification of PRE^{-A} complexes. PRE^{-A} complexes for smFRET experiments were assembled using 30S subunits purified from wild-type *E. coli* strain BW25113 and L1- and L9-labeled 50S subunits derived from a variant of strain BW25113 as described[7,55]. A mixture of 30 pmol biotin-mRNA, 20 pmol deacylated tRNA and 15 pmol 30S subunits, in a total reaction volume of 30 µl of Ribosome Assembly Buffer (50 mM Tris hydrochloride, $pH_{25\,°C}$ 7.5, 70 mM ammonium chloride, 30 mM potassium chloride, 6 mM 2-mercaptoethanol and 7 mM magnesium chloride), was incubated for 10 min at 37 °C. L1- and L9-labeled 50S subunits (10 pmol) were then added to the reaction followed by an additional incubation for 20 min at 37 °C. The reaction was then diluted to 100 µl with Tris-polymix buffer (50 mM Tris acetate, $pH_{25\,°C}$ 7.0, 100 mM potassium chloride, 5 mM ammonium acetate, 0.5 mM calcium acetate, 0.1 mM ethylenediamine tetraacetic acid, 10 mM 2-mercaptoethanol, 5 mM putrescine dihydrochloride and 1 mM spermidine, free base) containing 26 mM magnesium acetate to bring the final concentration of magnesium ions to 20 mM. The resulting PRE^{-A} complexes were then purified by 10–40% (w/v) sucrose density gradient ultracentrifugation[4,6].

smFRET experiments and data analysis. smFRET experiments were done in Tris-polymix buffer containing 15 mM magnesium acetate and supplemented with an oxygen-scavenging system (300 µg ml^{-1} glucose oxidase, 40 µg ml^{-1} catalase and 1% (w/v) β-D-glucose)[4,7,58] and a triplet-state quencher cocktail (1 mM 1,3,5,7-cyclooctatetraene (Sigma-Aldrich) and 1 mM 3-nitrobenzyl alcohol (Fluka))[59]. smFRET versus time trajectories were recorded using a laboratory-built, prism-based TIRF microscope with a 532-nm diode-pumped solid-state laser as an excitation source and an electron-multiplying charge-coupled device camera operating at a time resolution of 10 frames s^{-1}, unless otherwise specified, as a detector[6]. Each smFRET trajectory was idealized by hidden Markov modeling using the vbFRET software package (http://vbfret.sourceforge.net/)[60]. With the exception of $PRE^{-A}_{fMet\text{-}2}$, PRE^{-A}_{Anti} and PRE^{-A}_{Acc}, dwell times spent in GS1 before transitioning to GS2 and in GS2 before transitioning to GS1 were extracted from the idealized smFRET trajectories and the lifetimes of GS1 and GS2 were determined from exponential fits to the corresponding one-dimensional dwell-time histograms. $k_{GS1\rightarrow GS2}$ and $k_{GS2\rightarrow GS1}$ were calculated by taking the inverse of the lifetimes of GS1 and GS2, respectively, and correcting for the rate of photobleaching from each state[6,7]. For the smFRET trajectories recorded for $PRE^{-A}_{fMet\text{-}2}$, PRE^{-A}_{Anti} and PRE^{-A}_{Acc}, which had extended dwell times in GS1, a dwell-time analysis slightly modified from that described above was used. For these PRE^{-A} complexes, the slow $k_{GS1\rightarrow GS2}$ was calculated by the following procedure: (i) assuming a two-state GS1↔GS2 equilibrium model; (ii) calculating the corresponding K_{eq} from the ratio of GS1 and GS2 occupancies (K_{eq} = (occupancy of GS2) / (occupancy of GS1)); (iii) calculating the lifetime of GS2, and the corresponding $k_{GS2\rightarrow GS1}$, from a standard dwell-time analysis as described above and (iv) setting $k_{GS1\rightarrow GS2} = K_{eq} \times k_{GS2\rightarrow GS1}$. Detailed descriptions and references for all materials and methods can be found in the **Supplementary Methods**.

51. Alberts, B.M. & Frey, L. T4 bacteriophage gene 32: a structural protein in the replication and recombination of DNA. *Nature* **227**, 1313–1318 (1970).
52. Milligan, J.F., Groebe, D.R., Witherell, G.W. & Uhlenbeck, O.C. Oligoribonucleotide synthesis using T7 RNA polymerase and synthetic DNA templates. *Nucleic Acids Res.* **15**, 8783–8798 (1987).
53. Wyatt, J.R., Chastain, M. & Puglisi, J.D. Synthesis and purification of large amounts of RNA oligonucleotides. *Biotechniques* **11**, 764–769 (1991).
54. Sternberg, S.H., Fei, J., Prywes, N., McGrath, K.A. & Gonzalez, R.L. Jr. Translation factors direct intrinsic ribosome dynamics during translation termination and ribosome recycling. *Nat. Struct. Mol. Biol.* **16**, 861–868 (2009).
55. Fei, J. *et al.* A highly-purified, fluorescently-labeled *in vitro* translation system for single-molecule studies of protein synthesis. *Methods Enzymol.* **472**, 221–259 (2010).
56. Lee, C.P., Mandal, N., Dyson, M.R. & RajBhandary, U.L. The discriminator base influences tRNA structure at the end of the acceptor stem and possibly its interaction with proteins. *Proc. Natl. Acad. Sci. USA* **90**, 7149–7152 (1993).
57. Mandal, N., Mangroo, D., Dalluge, J.J., McCloskey, J.A. & Rajbhandary, U.L. Role of the three consecutive G:C base pairs conserved in the anticodon stem of initiator tRNAs in initiation of protein synthesis in *Escherichia coli*. *RNA* **2**, 473–482 (1996).
58. Stone, M.D. *et al.* Stepwise protein-mediated RNA folding directs assembly of telomerase ribonucleoprotein. *Nature* **446**, 458–461 (2007).
59. Gonzalez, R.L. Jr., Chu, S. & Puglisi, J.D. Thiostrepton inhibition of tRNA delivery to the ribosome. *RNA* **13**, 2091–2097 (2007).
60. Bronson, J.E., Fei, J., Hofman, J.M., Gonzalez, R.L. Jr. & Wiggins, C.H. Learning rates and states from biophysical time series: a Bayesian approach to model selection and single-molecule FRET data. *Biophys. J.* **97**, 3196–3205 (2009).

doi:10.1038/nsmb.2098